Geol. Mag. **152** (*6*), *2015, pp. 1057–1072.* © *Cambridge University Press 2015*
doi:10.1017/S0016756815000138

Geochronology, geochemistry, and geological implications of late Carboniferous – early Permian mafic and felsic intrusive rocks from Urad Zhongqi, western Inner Mongolia

YINGDE WANG, FENGYUE SUN*, LIANG LI, RUIHUA LI, JIAN WANG & WEI XIN

College of Earth Sciences, Jilin University, 2199 Jianshe Street, Changchun 130061, PR China

(*Received* 15 December 2014; *accepted* 3 March 2015; *first published online* 27 April 2015)

Abstract – The mafic and felsic Haertaolegai intrusions crop out in Urad Zhongqi, western Inner Mongolia and are dominated by monzogranite, porphyritic granite, and gabbroic diorite intrusions. We investigate the tectonic setting, geochronology, and anorogenic characteristics of the western Inner Mongolia through field investigation, microscopic and geochemical analyses of samples from the Haertaolegai bimodal intrusions and laser ablation multi-collector inductively coupled plasma mass spectrometry (LA-MC-ICP-MS) zircon U–Pb dating of gabbroic diorite and adakitic granites. Petrographic and geochemical studies of the bimodal intrusions indicate that the gabbroic diorites formed from a primary magma generated by the partial melting of lithospheric mantle material that had previously been modified by subduction-related fluids. The felsic rocks are high-K calc-alkaline and metaluminous, have characteristics of adakitic rocks and were generated during the partial melting of juvenile crustal material. Zircon U–Pb dating indicates that the felsic portion of this pluton was emplaced during late Carboniferous – early Permian time, with the mafic portion of the pluton emplaced during early Permian time. The zircons of adamellites have εHf(t) values and T_{DM2} ages of +1.0 to +2.7 and 1032–1128 Ma, respectively, suggesting that they formed from magmas generated by partial melting of juvenile Mesoproterozoic lower crust. These data, combined with the geology of the region, indicate that the late Carboniferous – early Permian bimodal intrusive rocks in western Inner Mongolia record a transitional period from collisional compression to post-collisional extension. These results indicate that the Paleo-Asian Ocean in western Inner Mongolia closed before 300 Ma.

Keywords: Adakitic rocks, bimodal intrusive rocks, western Inner Mongolia, Paleo-Asian Ocean.

1. Introduction

As one of the largest Phanerozoic sites of juvenile crustal formation and metallogenic belt in the world, the Central Asia Orogenic Belt (CAOB) has attracted much attention from geoscientists in the last few decades (Wang & Liu, 1986; Şengör, Natal'in & Burtman, 1993; Şengör & Natal'in, 1996; Jahn, Wu & Chen, 2000; Heubeck, 2001; Xiao *et al.* 2003, 2009; Windley *et al.* 2007; Jahn *et al.* 2009). The Xing'an–Mongolia Orogenic Belt (XMOB) is one of its important tectonic components. The Urad Zhongqi area forms the north-western part of Inner Mongolia and is located in the eastern CAOB within the western XMOB (Xu *et al.* 2014). The tectonism in this region records the evolution of the Paleo-Asian Ocean and the Palaeozoic collision between the North China and Siberian plates. This makes the area an ideal site to study the closure of the Paleo-Asian Ocean and accretion-type orogenesis.

Several issues dealing with the Palaeozoic evolution of the Paleo-Asian Ocean between the North China Craton and Mongolia Blocks are still controversial, especially the location of suture zone and the timing of the final oceanic closure. Ophiolites with various ages have been identified within different parts of the XMOB. The presence of these ophiolites, in addition to the available geological and palaeomagnetic data (Shao, 1991; Tang 1990, 1992; Xu & Chen, 1993, 1997; Xu & Charvet, 2010; Xu *et al.* 2013; Zhao *et al.* 2013), have led to the development of several models of the timing and location of the collision between the Siberian and North China plates in the central–western part of Inner Mongolia, including models involving the closure of the Paleo-Asian Ocean during Late Devonian – early Carboniferous time, whereas other models have suggested that closure occurred during late Permian time (Wang, 1996; Chen *et al.* 2000; Xiao *et al.* 2003, 2009; Windley *et al.* 2007; Jian *et al.* 2008; Chen, Jahn & Tian, 2009; Jian, Liu & Kröner, 2010).

Certain types of magmatic activity can provide useful guides to specific tectonic regimes, for example, the association of A-type granites, alkaline rocks and shoshonitic rocks with extensional environments (Seo, Choi & Oh, 2010; Yang *et al.* 2005). Recognition of some special rocks, in particular those with significance indicating tectonic setting, is therefore critical for further understanding of the tectonic evolution of the XMOB. In the current study, we report new zircon laser ablation inductively coupled plasma mass spectrometry (LA-ICP-MS) U–Pb and whole-rock geochemical data for late Carboniferous – early Permian bimodal intrusive rocks, mainly composed of adakitic granites and gabbroic diorite within western Inner Mongolia, NW China. These data provide evidence for the late

*Author for correspondence: sunfengyue2013@126.com

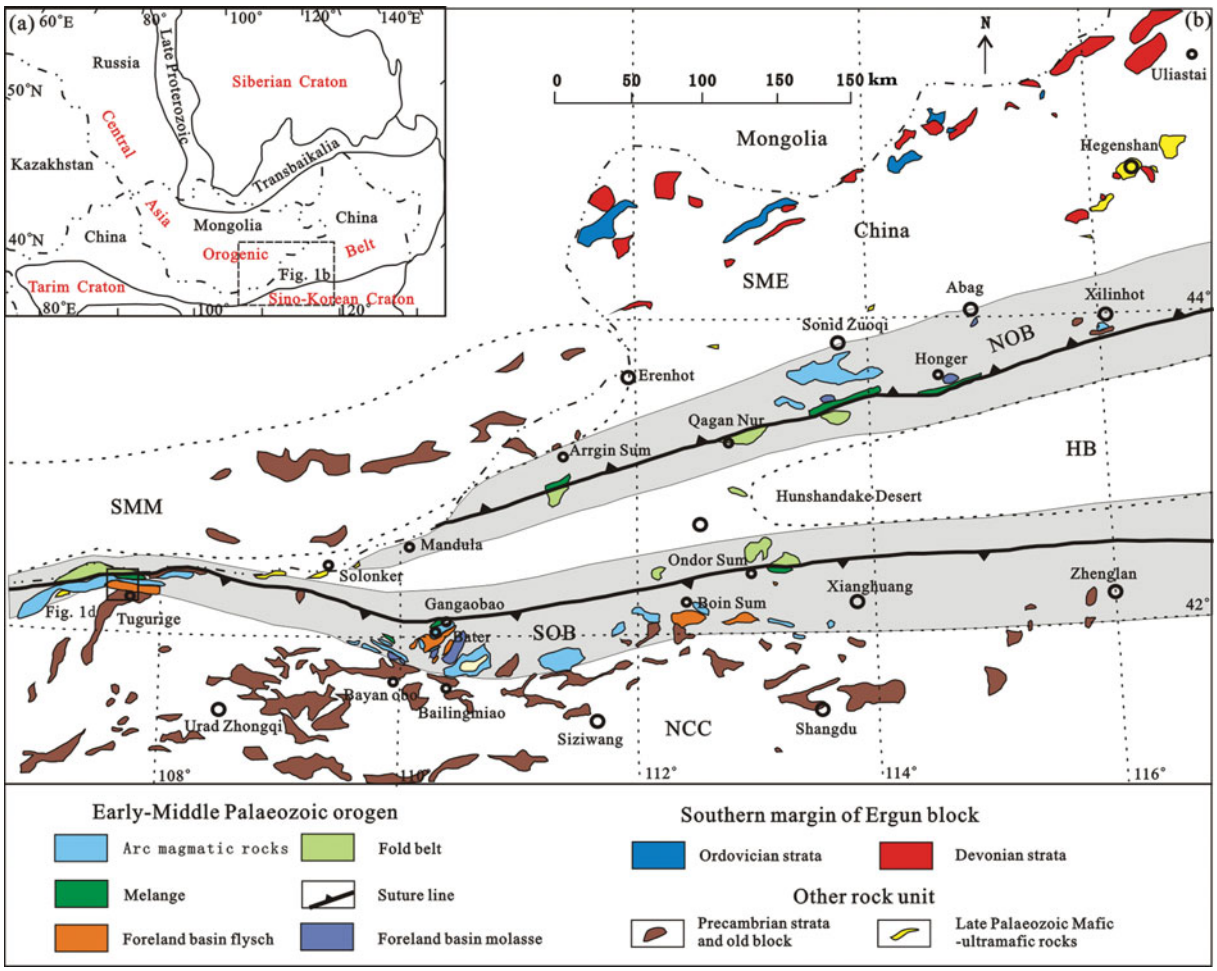

Figure 1. (Colour online) (a) Tectonic framework of the North China – Mongolia segment of the Central Asian Orogenic Belt (modified after Jahn, 2004). (b) Tectonic sketch map of western Inner Mongolia (after Xu *et al.* 2013). (c) Sketch geological map of northern North China showing the distribution of Palaeozoic magmatic rocks (modified after Zhang *et al.* 2011*a*). (d) Detailed geological map of the Haertaolegai area, showing the location of felsic and mafic rock samples analysed during this study.

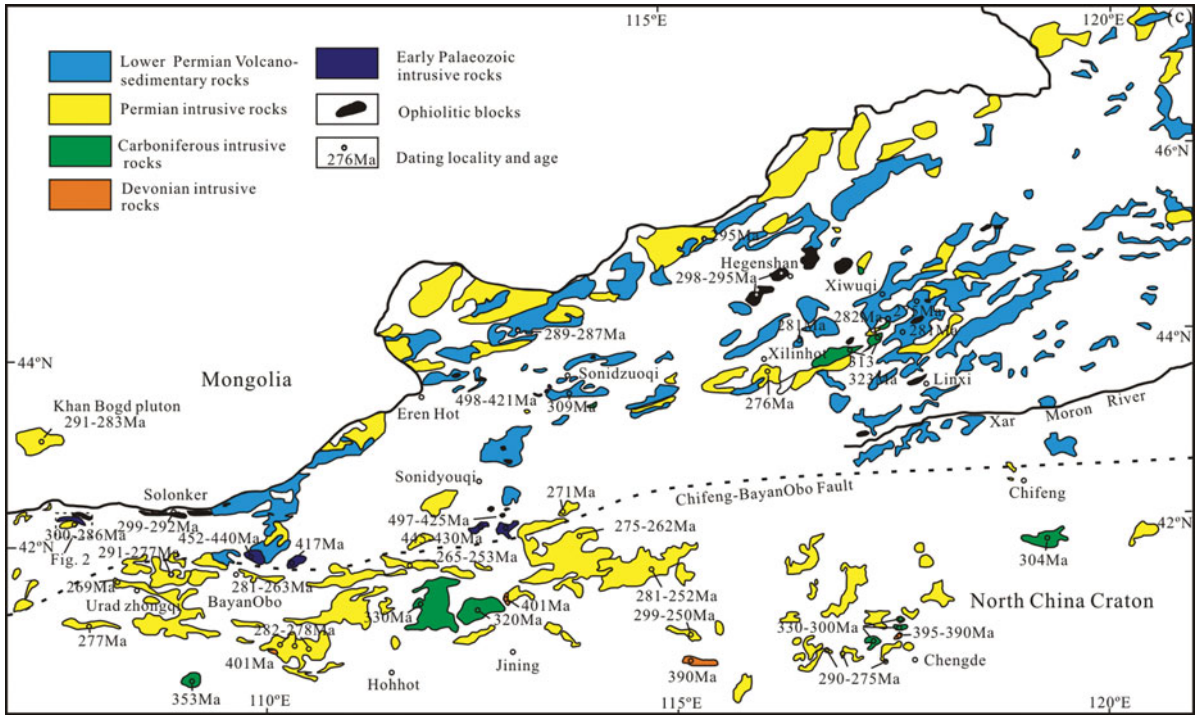

Figure 1. Continued

https://doi.org/10.1017/S0016756815000138 Published online by Cambridge University Press

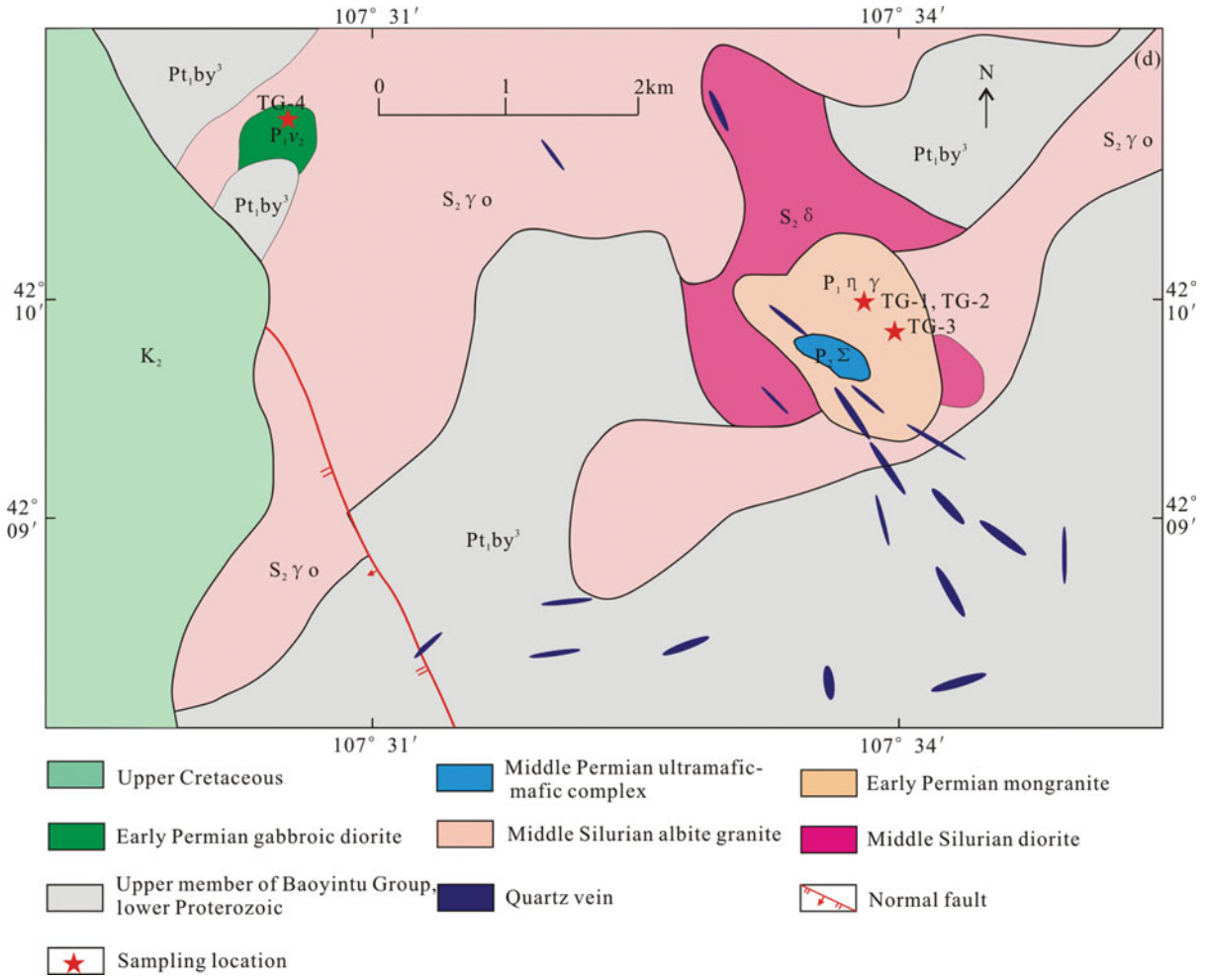

Figure 1. Continued

Carboniferous – early Permian tectonic setting of this area and the timing of closure of the Paleo-Asian Ocean. We conclude that the Haertaolegai late Carboniferous – early Permian bimodal intrusive rocks in western Inner Mongolia record a transitional period from collisional compression to post-collisional extension in western part of the XMOB.

2. Geological background and sample descriptions

The Haertaolegai mafic and felsic intrusions are located in the northwest margin of the North China Craton, within the western Xing'an–Mongolia Orogenic Belt. Western Inner Mongolia is split into the following six tectonic units: the North China Craton (NCC); the Southern Orogenic Belt (SOB); the Hunshandake Block (HB); the Northern Orogenic Belt (NOB); the South Mongolia microcontinent (SMM); and the southern margin of the Ergun Block (SME) (Xu *et al.* 2013). Solonker suture zone separates two opposite-facing continental blocks (Jian, Liu & Kröner, 2010). The northern block includes the SMM (Badarch, Cunningham & Windley, 2002) and the northern orogen (early – early late Palaeozoic) in northern China (Jian *et al.* 2008; Xu *et al.* 2013). The southern block comprises the southern orogen (early Palaeozoic) and the northern NCC (Jian, Liu & Kröner, 2010; Xu *et al.* 2013). These two blocks behaved as the combined North China – Mongolian plate subsequent to the closure of the Paleo-Asian Ocean (Davis *et al.* 2001; Zhang *et al.* 2010, 2012). The study area is located within the SOB, adjacent to the SMM to the north and the NCC to the south (Fig. 1a, b).

During late Palaeozoic time, the northern NCC experienced several magmatic events (Fig. 1c), such as Middle Devonian mafic and alkaline intrusions, Carboniferous foliated calc-alkaline plutons, early Permian high-K calc-alkaline I-, S- and A-type granitoids, and the latest Permian – Early Triassic high-K calc-alkaline–alkaline intrusive rocks (Zhang *et al.* 2011*a*).

The small stock-like Haertaolegai intrusion was emplaced within metamorphic basement of the Palaeoproterozoic Baoyintu Group which divided into three petrofabrics (from bottom to top): quartzite-granulite formation (Pt_1by^1); garnet schist formation (Pt_1by^2); and quartzite-marble formation (Pt_1by^3). The intrusion also intrudes an early Silurian albite granite with LA-ICP-MS zircon U–Pb age of 426 Ma (unpublished data). The Baoyintu Group is composed mainly of quartzite, quartz-rich micaschist, staurolite–kyanite schist intercalated with marble and plagioclase amphibole schist, dolomitic marble, staurolite–garnet

https://doi.org/10.1017/S0016756815000138 Published online by Cambridge University Press

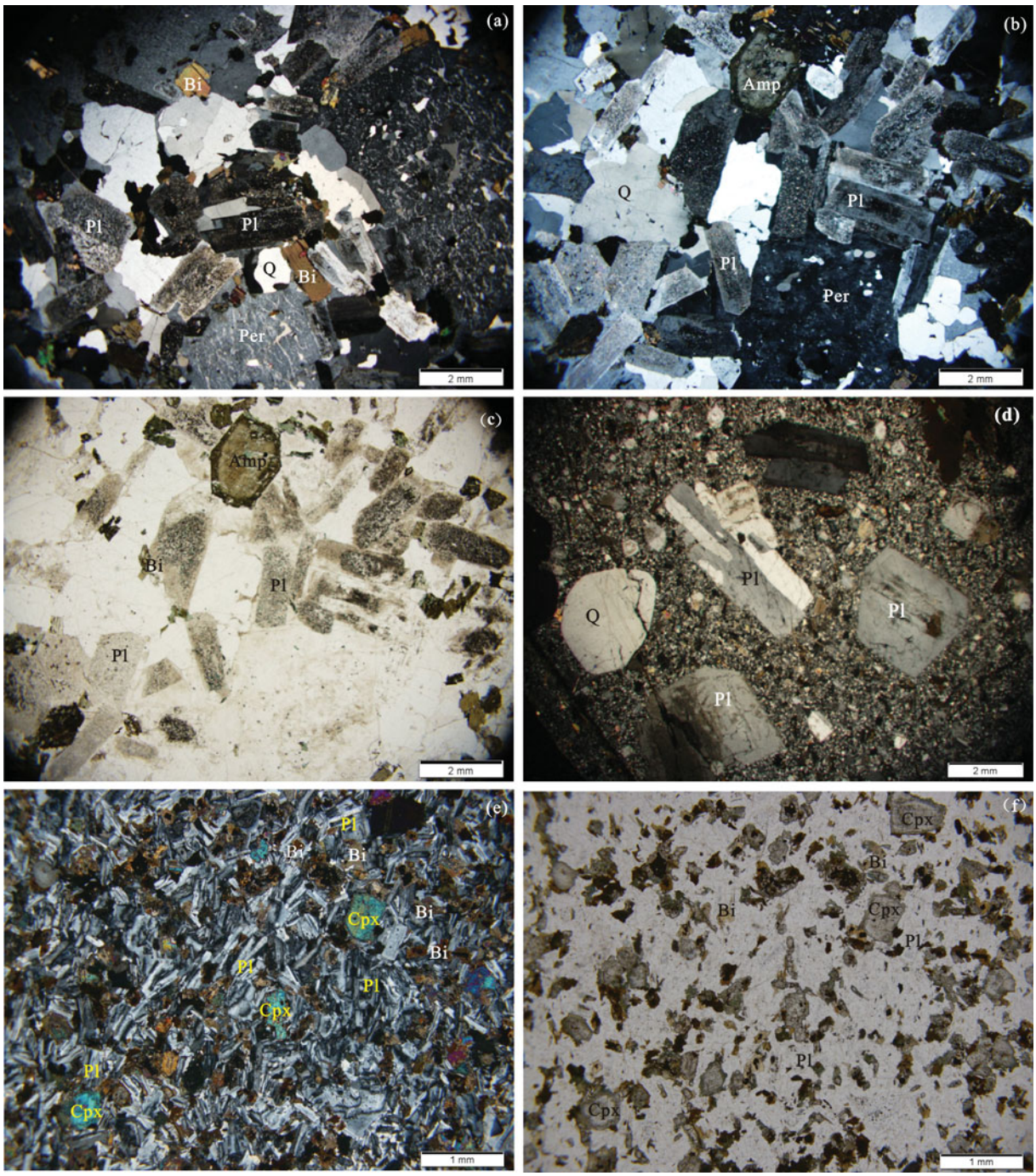

Figure 2. (Colour online) Representative photomicrographs of the mafic and felsic rocks analysed during this study, showing typical textures and internal structures: (a) adamellite (TG-1), cross-polarized light; (b) adamellite (TG-2), cross-polarized light; (c) adamellite (TG-2), single-polarized light; (d) granitic porphyry (TG-3), cross-polarized light; (e) gabbroic diorite (TG-4), cross-polarized light; (f) gabbroic diorite (TG-4), single-polarized light. Amp – amphibole; Bi – biotite; Cpx – clinopyroxene; Per – perthite; Pl – plagioclase; Q – quartz.

mica schist, biotite-bearing amphibole schist, leptynite and actinolite schist. A whole-rock Sm–Nd isochron age of 2485 ± 128 Ma from the plagioclase amphibole schist is interpreted as the age of the Baoyintu Group (Xu *et al.* 2000, 2013). The area contains well-developed NEE–SWW- and nearly E–W-trending faults and numerous intrusive rocks, including a Silurian albite granite, a Permian ultramafic–mafic complex, and a Permian monzogranite. The early Permian granite in this area is dominated by porphyritic adamellite and porphyritic granite phases, whereas the mafic rocks in the study area are dominantly gabbroic diorites (Fig. 1d).

The adamellite (samples TG-1 and TG-2) within the study area is pale red and porphyritic, has a granitic texture and contains plagioclase (*c.* 45 %), perthite (*c.* 25 %), quartz (*c.* 20 %), biotite (*c.* 5 %) and amphibole (*c.* 3 %) with accessory zircon, apatite, titanite, and Fe–Ti oxides (<2 %) (Fig. 2a–c). This phase of the intrusion is cross-cut by quartz veins and

https://doi.org/10.1017/S0016756815000138 Published online by Cambridge University Press

porphyritic granite dykes. The latter consist of light flesh-pink-coloured porphyritic granite (sample TG-3) that is massive and contains plagioclase and quartz phenocrysts (20–25 %) within a microgranular matrix of K-feldspar, quartz, plagioclase and biotite (Fig. 2d).

The gabbroic diorite (sample TG-4) within the mafic part of the pluton is gabbro textured and contains plagioclase (*c.* 70 %), clinopyroxene (*c.* 12 %), biotite (*c.* 10 %) and hornblende (*c.* 5 %) with accessory magnetite, apatite, zircon, and epidote (*c.* 5 %) (Fig. 2e, f).

3. Analytical methods

3.a. Zircon U–Pb dating

The samples used for zircon U–Pb dating were conventionally crushed and separated using heavy liquids and a magnetic separator at the Langfang Regional Geological Survey, Hebei Province, China. Approximately 250 zircons were handpicked from each sample and were embedded within resin discs under a binocular microscope before being polished to expose grain centres. Transmitted and reflected light images were captured using a microscope, and cathodoluminescence (CL) imaging was undertaken using a JEOL scanning electron microscope. LA-ICP-MS zircon U–Pb analysis of TG-1 and TG-2 samples was conducted using an Agilent 7500a ICP-MS instrument equipped with a 193 nm laser at the State Key Laboratory of Continental Dynamics, Northwestern University, Xi'an, China, using a 30 μm spot diameter. Details of the analytical technique are described by Yuan *et al.* (2004), common Pb concentrations were evaluated following Andersen (2002) and ISOPLOT version 3.0. (Ludwig, 2003) was used for age calculations and for constructing concordia diagrams.

LA-ICP-MS U–Pb analyses of zircons separated from TG-3 and TG-4 samples were performed using an Agilent 7500a ICP-MS instrument equipped with a 193 nm laser at the State Key Laboratory of Geological Processes and Mineral Resources, China University of Geosciences, Wuhan, China using a 91500 standard zircon as an external standard for age calibration and a NIST SRM 610 silicate glass standard for instrument optimization. This analysis used a 30 μm spot size with instrument parameters and detailed analytical procedures identical to those described by Liu *et al.* (2008). The ICPMS DataCal version 6.7 (Liu *et al.* 2008) and Isoplot version 3.0 (Ludwig, 2003) programs were used for data reduction, with correction for common Pb undertaken following Andersen (2002). Errors on individual LA-ICP-MS analyses are quoted at the 1σ level, whereas errors on pooled ages are quoted at the 95 % (2σ) confidence level. The dating results are presented in the online Supplementary Material (Table S1, available at http://journals.cambridge.org/geo).

3.b. Major and trace element determination

Major and trace element compositions of the mafic and felsic samples were determined by X-ray fluorescence spectrometer (XRF; Philips PW2404) and plasma mass spectrometer (ICP-MS; ELEMENT 1), respectively, at the Geological Analysis and Research Centre of Nuclear Industry of China, Beijing, China. Major elements concentrations were determined using a Philips PW-2404 X-fluorescence spectrometer, and all trace and rare Earth element (REE) concentrations, with the exception of Sb and Bi, were determined by ICP-MS and an Element-2 mass spectrometer. Sb and Bi concentrations were determined by atomic fluorescence spectrometry using a double-channel AFS-2202 spectrometer. The analytical precision for major elements is better than 5 %, and trace element concentrations have relative deviations of <5 % for concentrations of >10 ppm and of <10 % for other concentrations. The detailed analysis process is described by Qu, Hou & Li (2004).

3.c. *In situ* zircon Hf isotope analysis

In situ zircon Hf isotope analysis was undertaken using a Neptune Plus MC-ICP-MS instrument equipped with a 193 nm laser at the state Key Laboratory of Geological Processes and Mineral Resources, China University of Geosciences, Wuhan, China using the instrumental conditions and data acquisition procedures described by Hu *et al.* (2012). A 91500 standard zircon was used as an external standard, and a spot size of 44 μm and a laser repetition rate of 6–8 Hz at 100 mJ were used during analysis. $^{179}Hf/^{177}Hf$ and $^{173}Yb/^{171}Yb$ ratios were used to calculate the mass bias of Hf (βHf) and Yb (βYb), and the interference of ^{176}Yb on ^{176}Hf was corrected by measuring the interference-free ^{173}Yb isotope and using $^{176}Yb/^{173}Yb = 0.79639$ (Fisher *et al.* 2014) to calculate $^{176}Yb/^{177}Hf$ values. The relatively minor interference of ^{176}Lu on ^{176}Hf was corrected by measuring the intensity of the interference-free ^{175}Lu isotope and using the recommended $^{176}Lu/^{175}Lu = 0.02656$ value (Blichert-Toft *et al.* 1997) to calculate $^{176}Lu/^{177}Hf$. Finally, the mass bias of Yb (βYb) was used to calculate the mass fractionation of Lu. The program ICPMSDataCal (Liu *et al.* 2010) was used to perform off-line selection and mass bias calibrations, and to integrate analyte signals.

4. Results

4.a. Zircon U–Pb ages

Zircons from both mafic and felsic samples are generally euhedral and colourless, and contain typical magmatic rhythmic banding and oscillatory zoning (Fig. 3). The granitic zircons are long to short prismatic and have mean crystal sizes of 100–200 μm, whereas the gabbroic diorite zircons are 80–120 μm long and have widths of 40–60 μm (Fig. 3). Some zircons have inherited cores that are commonly corroded, reflecting the influence of magmatism on the cores. The majority of zircons have highly variable Th (384–7171 ppm for mafic, 67–981 ppm for felsic) and U (755–4733 ppm for mafic, 86–2595 ppm for felsic)

https://doi.org/10.1017/S0016756815000138 Published online by Cambridge University Press

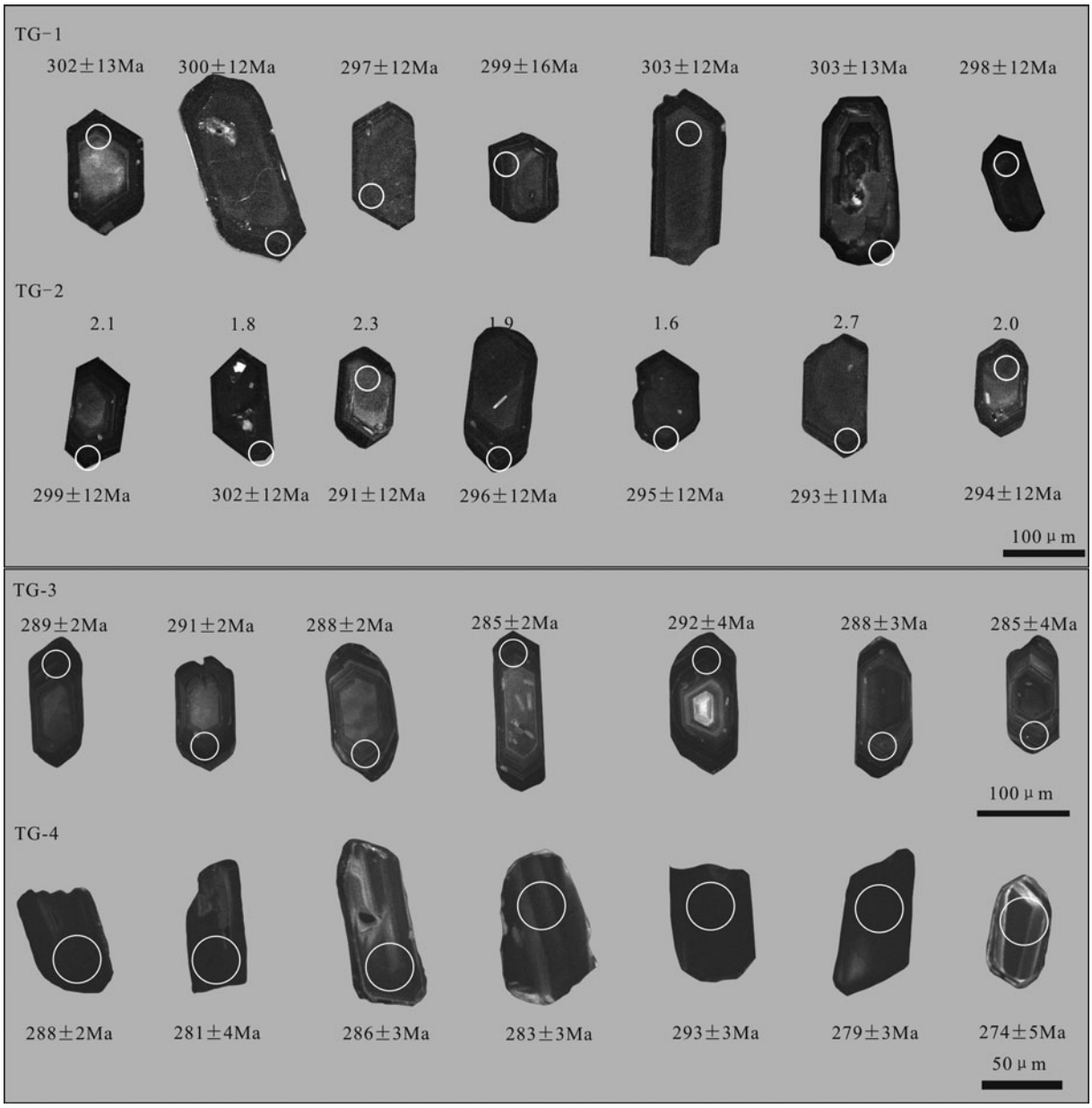

Figure 3. Cathodoluminescence (CL) images of zircons from mafic and felsic rocks analysed during this study. The numbers on the images indicate individual analysis spots, and the values below the images show zircon ages and εHf(t) values.

concentrations, yielding high Th/U ratios of 0.45–1.51 and 0.19–0.52 for mafic and felsic samples, respectively, all of which is indicative of a magmatic origin for these zircons (Hoskin & Schaltegger, 2003).

Adamellite samples TG-1 and TG-2 yielded weighted mean $^{206}Pb/^{238}U$ ages of 300 ± 6 (MSWD = 0.1; n = 20) and 297 ± 2 Ma (MSWD = 0.2; n = 21), respectively (Fig. 4a, b), which represent the timing of formation of the monzogranite intrusion. Sample TG-3 from the porphyritic granite dyke yielded a weighted mean $^{206}Pb/^{238}U$ age of 286 ± 3 Ma (MSWD = 4.1; n = 16; Fig. 4c) that is indicative of the timing of emplacement of the dyke. Finally, the 10 analyses of zircons from gabbroic sample TG-4 yielded a weighted mean $^{206}Pb/^{238}U$ age of 286 ± 4 Ma (MSWD = 3.6; n = 10; Fig. 4d).

4.b. Major and trace elements

The major and trace element compositions of the felsic rocks are given in the online Supplementary Material (Table S2, available at http://journals.cambridge.org/geo). The granitic samples have SiO_2 concentrations of 68.34–70.74 wt %, Al_2O_3 concentrations of 14.88–15.67 wt %, MgO concentrations of 0.73–1.05 wt %, Na_2O concentrations of 4.24–4.86 wt % and K_2O concentrations of 3.38–4.36 wt %, yielding Na_2O/K_2O ratios of 0.97–1.42 (Table S2). These samples have A/CNK (molar $Al_2O_3/(CaO + K_2O + Na_2O)$) ratios of 0.88–0.98, indicating that these are metaluminous granites (Fig. 5b; Maniar & Piccoli, 1989) and are classified as sub-alkaline in a total alkalis versus SiO_2 (TAS) diagram (Fig. 5a; Irvine & Baragar,

https://doi.org/10.1017/S0016756815000138 Published online by Cambridge University Press

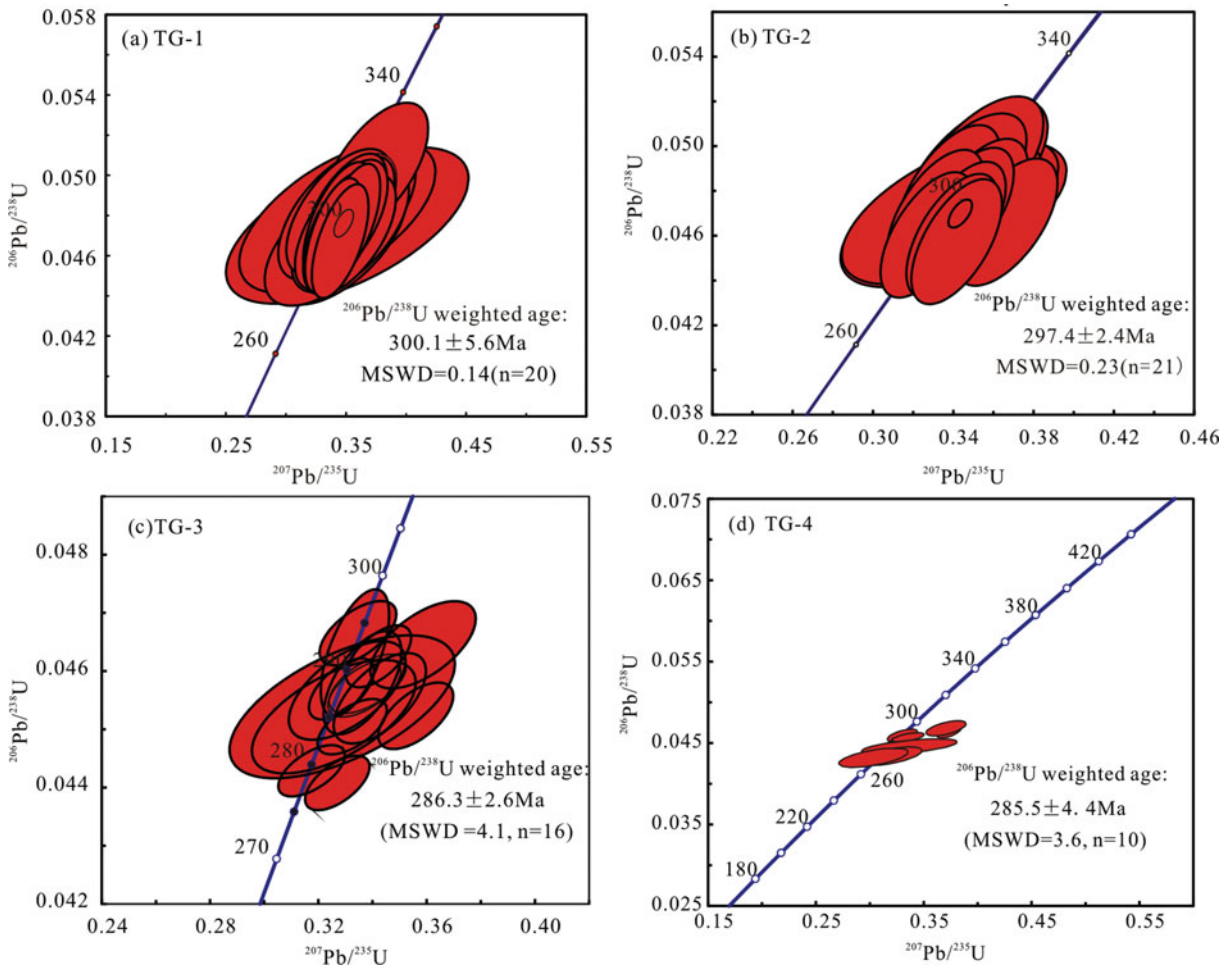

Figure 4. (Colour online) Zircon U–Pb concordia diagram for the mafic and felsic rocks analysed during this study.

1971). All of these samples are classified as high-K and calc-alkaline in a K_2O versus SiO_2 diagram (Fig. 5c). They are enriched with light rare Earth elements (LREEs) and large-ion lithophile elements (LILEs), are depleted in heavy REEs (HREEs) and high-field-strength elements (HFSEs) (Fig. 6a, b) and have $(La/Yb)_N$ ratios and Eu/Eu∗ values of 35.5–89.9 and 0.93–1.17, respectively. In addition, they have high Sr (521–736 ppm) and low Y (3.76–6.19 ppm) and Yb (0.22–0.60 ppm) concentrations, and are classified as adakites in Sr/Y versus Y and $(La/Yb)_N$ versus $(Yb)_N$ diagrams (Fig. 7a, b).

The samples from the mafic stock are generally classified as gabbroic diorites, and have SiO_2 concentrations of 55.21–56.13 wt %, with high total Fe_2O_3 (8.93–9.31 wt %), Al_2O_3 (15.98–16.63 wt %), MgO (3.72–4.55 wt %), K_2O (2.06–2.21 wt %) and CaO (6.67–7.24 wt %) concentrations and low TiO_2 (0.88–0.95 wt %) and P_2O_5 (0.27–0.42 wt %) concentrations. These samples are high-K and calc-alkaline, with A/CNK ratios of 0.81–0.99 (Fig. 5b). They are moderately enriched with LREEs ($(La/Yb)_N = 11.0–14.2$) and have weakly negative Eu anomalies (Eu/Eu∗ = 0.87–0.98; Fig. 6a), and are enriched with LILEs (such as Sr, Ba, and Rb) relative to the LREEs and HFSEs (such as Nb, Ta, P and Ti) within primitive-mantle-normalized multi-element variation diagrams.

4.c. Zircon Hf isotopes

The results of *in situ* Hf isotopic analysis of zircons from adamellite sample TG-2 are listed in Table 1 and depicted in Figure 8a,b.

The initial $^{176}Hf/^{177}Hf$ ratios of zircons from the adamellite (TG-2) range from 0.282134 to 0.282219, with εHf(t) values and corresponding Hf two-stage model ages (T_{DM2}) of 1.0–2.7 and 1032–1128 Ma consistent with those from the XMOB (Fig. 8a; Yang *et al.* 2006).

5. Discussion

5.a. Petrogenetic relationship between mafic and felsic rocks

The relationship between the early Permian mafic and felsic rocks in the study area can be determined using field relationships and geochemical data. First, the granitic and mafic magmas were intruded independently, and the granitic intrusions are exposed over a

https://doi.org/10.1017/S0016756815000138 Published online by Cambridge University Press

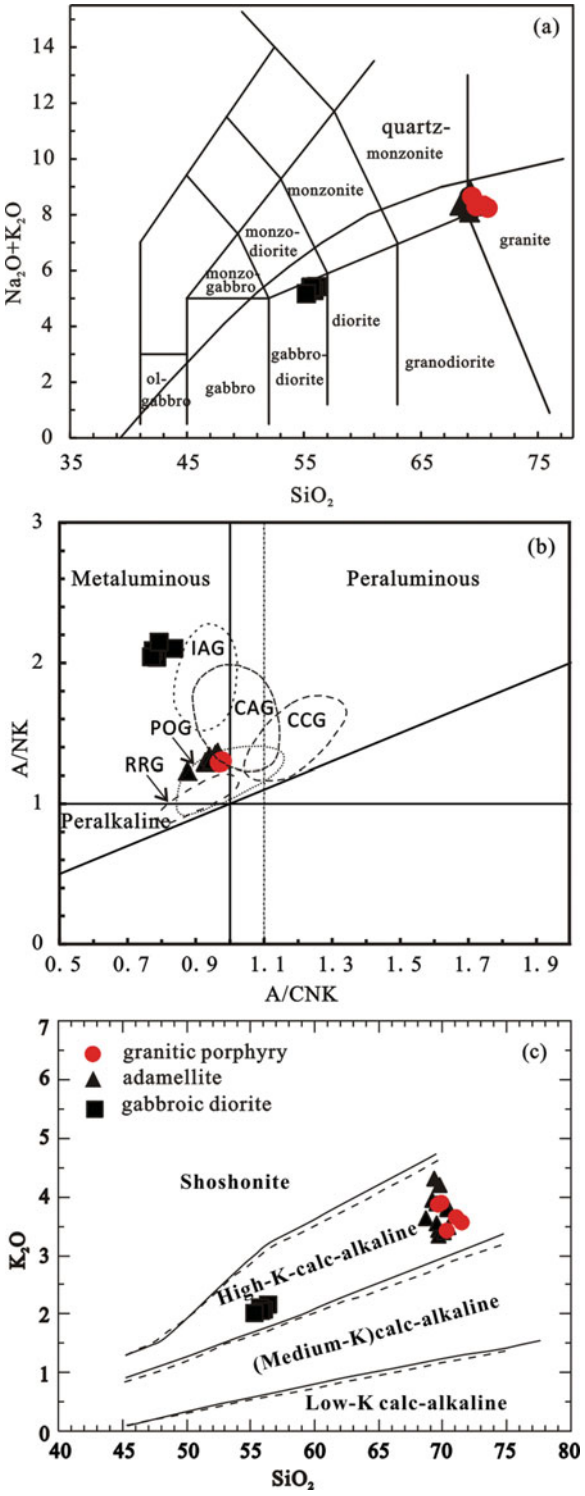

Figure 5. (Colour online) Chemical compositions of adamellite, granitic porphyry and gabbroic diorite rocks analysed during this study. (a) SiO_2 versus total alkali ($Na_2O + K_2O$) concentrations. (b) A/CNK versus A/NK. IAG – island-arc granotoid; CAG – continental arc granotoid; CCG – continental collisional granotoid; POG– post-orogenic granotoid; RRG – rift ridge grantoid (Dong *et al.* 2012). (c) SiO_2 versus K_2O. The boundary lines in the SiO_2 versus ($Na_2O + K_2O$), SiO_2 versus K_2O and A/CNK versus A/NK diagrams are from Irvine & Baragar (1971), Peccerillo & Taylor (1976), and Maniar & Piccoli (1989), respectively.

larger area than the coeval mafic intrusions. Second, the presence of a compositional gap between the mafic and granitic rocks (Fig. 5a) suggests that they formed independently. Finally, the gabbroic diorites have higher total REE abundances than the coeval granitoids (Fig. 6a, c), which is inconsistent with a fractional crystallization relationship between the mafic and felsic rocks. These features indicate that the early Permian granitic and mafic rocks have independent origins.

5.b. Petrogenesis of the mafic rocks and magma source

The early Permian mafic rocks in the study area have low SiO_2 concentrations (55.21–56.13 wt %), high Ni (10.2–17.2 ppm), Co (24.5–29.2 ppm), Sc (19.1–23.9 ppm) and Cr (46.2–73.9 ppm) concentrations, and high Mg numbers (45.0–50.2; Mg no. = 100 $Mg/(Mg + TFe^{2+})$) and Na_2O/K_2O ratios (1.5–1.6; Table S2, available at http://journals.cambridge.org/geo) that suggest these rocks formed from a primary basaltic magma that was derived from the partial melting of lithospheric mantle material (Frey & Prinz, 1978). In addition, relevant experimental petrology had proved that high-Mg-number adakitic rocks cannot be produced by partial melting of basaltic rocks (Rapp & Watson, 1995). This further suggests that the magma source for the gabbroic diorites should be upper mantle, but not lower crust or crust–mantle transitional zone (Chen & Zhou, 2004). However, these mafic rocks are also significantly enriched with LILEs (e.g. Ba, Th, U) and LREEs and depleted in HFSEs (e.g. Nb, Ta, and Ti), as evidenced by chondrite-normalized REE and primitive-mantle-normalized trace element variation diagrams (Fig. 6c, d). These geochemical characteristics are consistent with formation from melts derived from a depleted mantle source that was metasomatized by subduction-related fluids (Abe, Arai & Yurimoto, 1998; Eiler *et al.* 2000; Grove *et al.* 2003), or from melts from a depleted mantle source that assimilated crustal materials during magma ascent and emplacement (Wilson, 1989; Yang *et al.* 2008).

In general, Nb/U and Ta/U ratios can be used as indices of crustal contamination. The mafic rocks in the study area have Nb/U and Ta/U ratios of 3.76–6.64 and 0.26–0.41, respectively, both of which are not only much lower than mid-ocean ridge basalt (MORB) and ocean island basalt (OIB) values (Nb/U = 47, Ta/U = 2.7; Hofmann, 1988), but are also lower than typical crustal values (Nb/U = 12.1, Ta/U = 1.1; Taylor & McLennan, 1995). Although the Nb/U and Ta/U ratios of these mafic rocks are similar to those of the upper continental crust (Nb/U = 8.9 and Ta/U = 0.2; Taylor & McLennan, 1995), their Sr concentrations (726–769 ppm; Table S2, available at http://journals.cambridge.org/geo) are much higher than that of continental crust in general (Sr = 280–348 ppm; Rudnick & Gao, 2003) and the upper continental crust (350 ppm; Taylor & McLennan, 1995;

https://doi.org/10.1017/S0016756815000138 Published online by Cambridge University Press

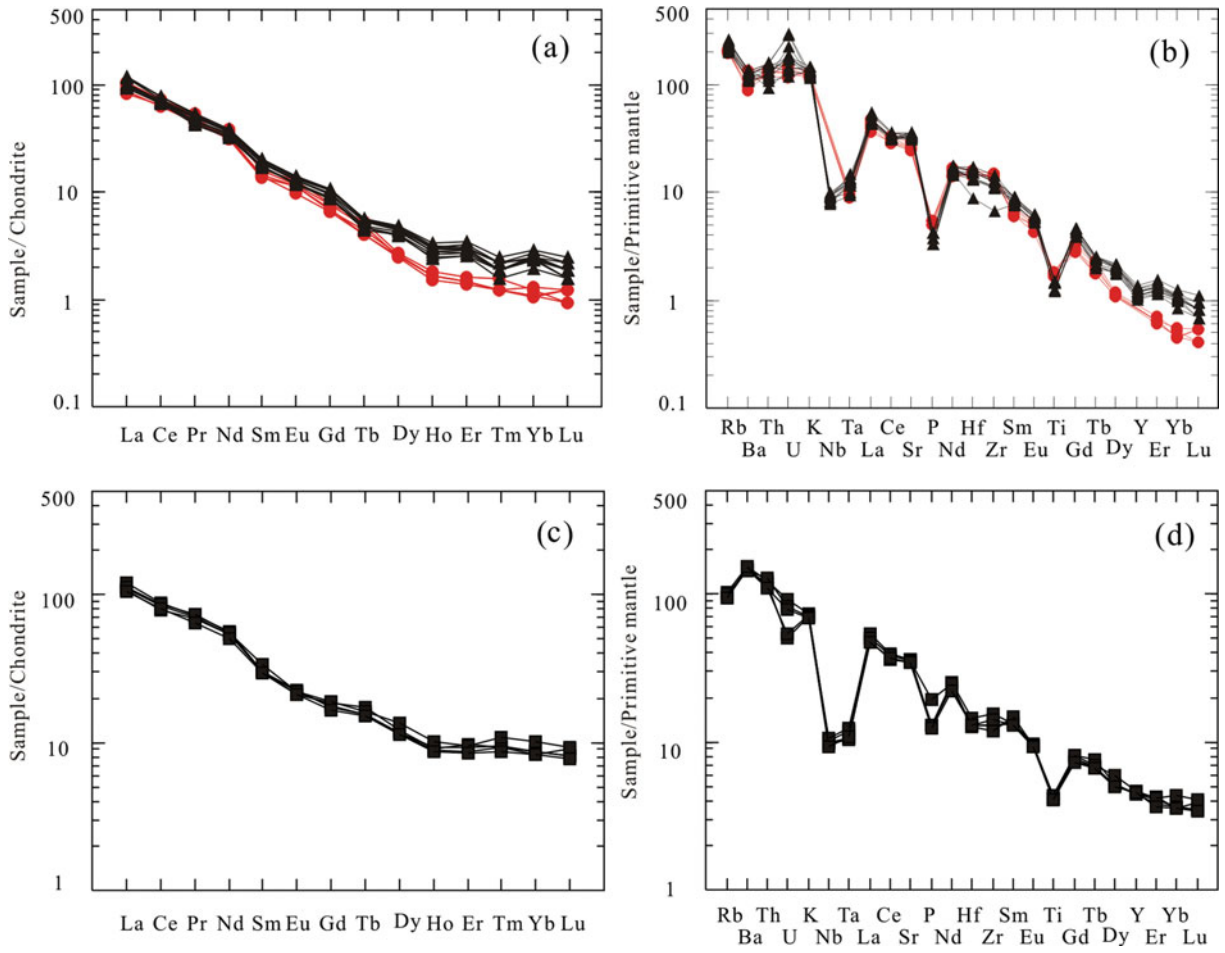

Figure 6. (Colour online) (a, c) Chondrite-normalized REE patterns and (b, d) primitive-mantle-normalized trace element spidergrams for the mafic and felsic rocks examined in this study. Chondrite and primitive mantle normalizing values are from Boynton (1984) and Sun & McDonough (1989), respectively. Symbols as for Figure 5c.

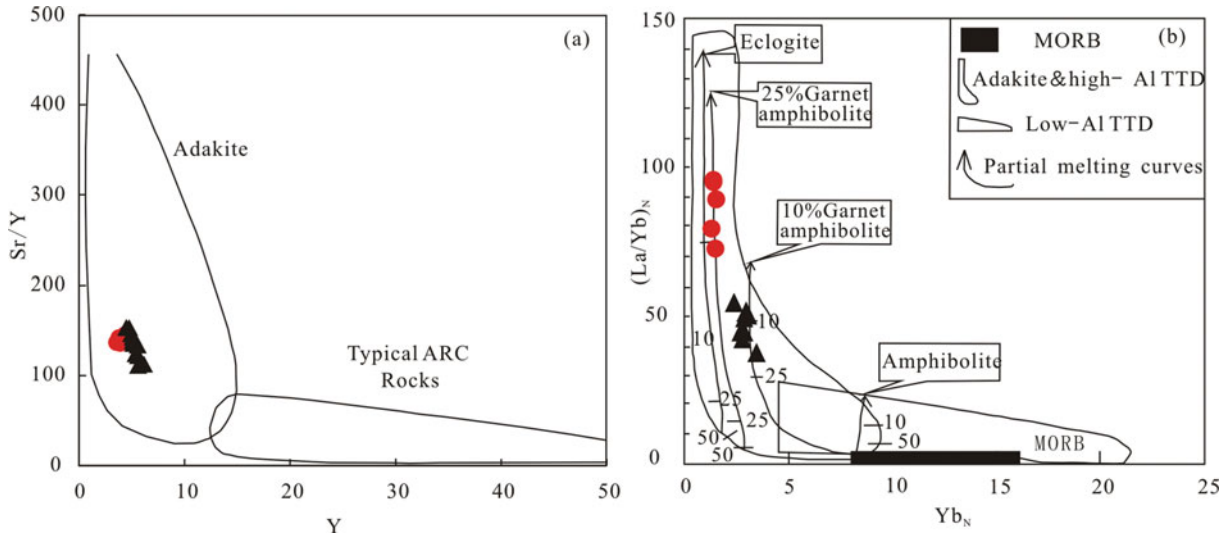

Figure 7. (Colour online) Plots of (a) Sr/Y versus Y and (b) $(La/Yb)_N$ versus $(Yb)_N$ for the adamellite and granitic porphyry rocks. Modified after Defant & Drummond (1990); adakite fields from Martin (1999).

267 ppm, Gao *et al.* 1998). In addition, the gabbroic diorites have higher La/Nb (4.55–5.09) and Ba/Nb (131–162) ratios than the continental crust, suggesting that the magmas that formed these rocks assimilated minimal crustal material during ascent and emplacement.

In summary, we suggest that the early Permian gabbroic diorites within the study area were derived from partial melting of lithospheric mantle material that was previously metasomatized by subducted slab-derived fluids.

https://doi.org/10.1017/S0016756815000138 Published online by Cambridge University Press

Table 1. Lu–Hf isotopic data for the adamellite rocks in the study area.

Sample	T (Ma)	$^{176}Yb/^{177}Hf$	$^{176}Lu/^{177}Hf$	$^{176}Hf/^{177}Hf$	$1\sigma_m$	$\varepsilon_{Hf}(0)$	$\varepsilon_{Hf}(t)$	1σ	$T_{DM1(Hf)}$	$T_{DM2(Hf)}$	$f_{Lu/Hf}$
TG-2-01	297	0.026536	0.000966	0.282651	0.000010	−4.3	2.1	0.7	850	1070	−0.97
TG-2-02	297	0.021472	0.000771	0.282656	0.000013	−4.1	2.3	0.7	838	1057	−0.98
TG-2-03	297	0.015035	0.000542	0.282668	0.000010	−3.7	2.7	0.6	817	1032	−0.98
TG-2-04	297	0.019470	0.000732	0.282643	0.000016	−4.6	1.8	0.8	857	1083	−0.98
TG-2-05	297	0.019419	0.000706	0.282637	0.000009	−4.8	1.6	0.6	865	1095	−0.98
TG-2-06	297	0.019727	0.000711	0.282644	0.000010	−4.5	1.9	0.6	855	1081	−0.98
TG-2-07	297	0.021851	0.000813	0.282648	0.000011	−4.4	2.0	0.7	852	1075	−0.98
TG-2-08	297	0.024570	0.000907	0.282668	0.000010	−3.7	2.7	0.6	825	1036	−0.97
TG-2-09	297	0.019777	0.000753	0.282628	0.000013	−5.1	1.3	0.7	878	1113	−0.98
TG-2-10	297	0.018996	0.000706	0.282656	0.000010	−4.1	2.3	0.6	838	1057	−0.98
TG-2-11	297	0.024908	0.000936	0.282663	0.000010	−3.9	2.5	0.6	833	1046	−0.97
TG-2-12	297	0.024104	0.000903	0.282634	0.000012	−4.9	1.5	0.7	872	1102	−0.97
TG-2-13	297	0.022088	0.000835	0.282648	0.000012	−4.4	2.0	0.7	851	1073	−0.97
TG-2-14	297	0.018806	0.000707	0.282620	0.000011	−5.4	1.0	0.7	888	1128	−0.98
TG-2-15	297	0.021690	0.000811	0.282624	0.000010	−5.2	1.1	0.7	884	1120	−0.98

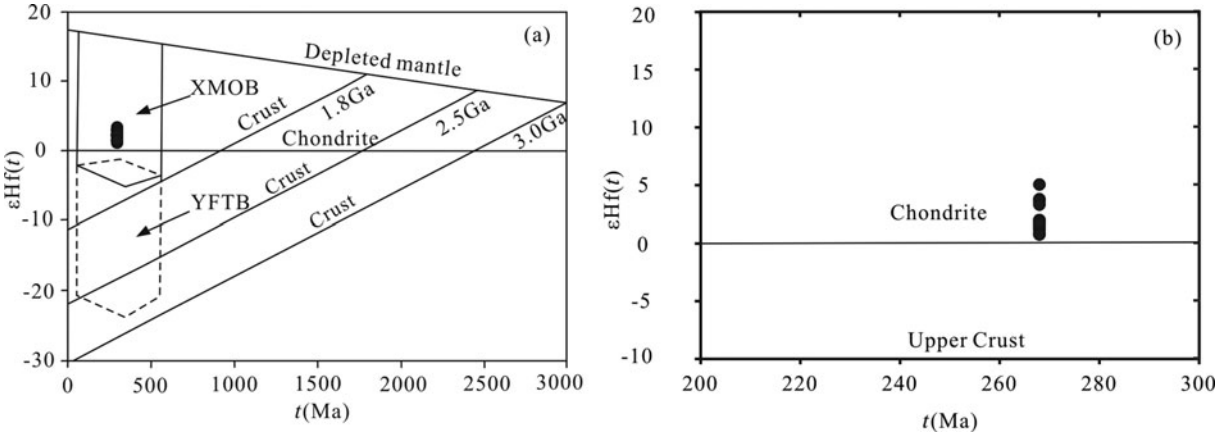

Figure 8. Correlations between Hf isotopic compositions and the formation ages of the adamellite (TG-2) in the study area. XMOB – Xing'an–Mongolia Orogenic Belt; YFTB – Yanshan Fold and Thrust Belt (Yang *et al.* 2006).

5.c. Petrogenesis of the felsic rocks and magma source

The geochemistry of the adamellite and porphyritic granite phases of the felsic Haertaolegai intrusion suggests they are adakitic (Defant & Drummond, 1990; Fig. 7a, b), as evidenced by their high SiO_2 (>56 wt %), Al_2O_3 (≥15 wt %), Na_2O (>3.5 wt %) and Sr (>400 ppm) and low Y (<18 ppm) and Yb (<1.9 ppm) concentrations.

Several genetic models have been proposed for adakitic rocks, including: (1) partial melting of subducting oceanic slab material (Defant & Drummond, 1990; Martin, 1999; Martin *et al.* 2005); (2) partial melting of thickened mafic lower continental crustal material (Atherton & Petford, 1993; Wareham, Millar & Vaughan, 1997; Zhang *et al.* 2001; Wang *et al.* 2005); (3) partial melting of delaminated lower continental crustal material (Kay & Kay, 1993; Xu *et al.* 2002; Gao *et al.* 2004); and (4) fractional crystallization of a parental basaltic magma (Castillo, Janney & Solidum, 1999; Macpherson, Dreher & Thirwall, 2006). The adakitic rocks within the felsic Haertaolegai intrusion have Na_2O concentrations (4.24–4.86 wt %) and Na_2O/K_2O ratios (0.97–1.42 with an average of 1.24) that are lower than those of adakitic rocks produced by partial melting of subducting oceanic slab material (Na_2O concentrations of 4.88 wt % and Na_2O/K_2O ratios of 2.5–6.5; Sajona, *et al.* 2000). In addition, adakitic rocks that form by partial melting of subducting oceanic slab material have low K_2O concentrations and Rb/Sr ratios (0.04–0.05), and high Mg numbers (Mg no. >47; Martin, 1999; Smithies, 2000) that contrast with the high K calc-alkaline adakitic rocks in the study area; the latter have high K_2O concentrations (3.46–4.36 wt %) and Rb/Sr ratios of 0.19–0.25. This indicates that the adakitic rocks within the Haertaolegai pluton were not produced by partial melting of subducting oceanic slab material.

The high SiO_2 concentrations (68.34–70.74 wt %) and Th/U ratios (2.11–4.37) and low MgO (0.73–1.05 wt %), Cr (14.9–35.4 ppm) and Ni concentrations (6.84–13.8 ppm) and Mg numbers (39.4–44.8) of these adakitic rocks are also inconsistent with melts derived from delaminated lower crustal material. Typically, such melts would have high Cr and Ni concentrations and low Th/U ratios, similar to melts derived from thickened lower continental crustal material. Adakitic rocks can also be produced by the low-pressure fractional crystallization of basaltic magmas (Castillo, Janney & Solidum, 1999; Gao *et al.* 2009). However, the low Cr and Ni concentrations of the adakitic rocks in the study area suggest that they are not the products of

https://doi.org/10.1017/S0016756815000138 Published online by Cambridge University Press

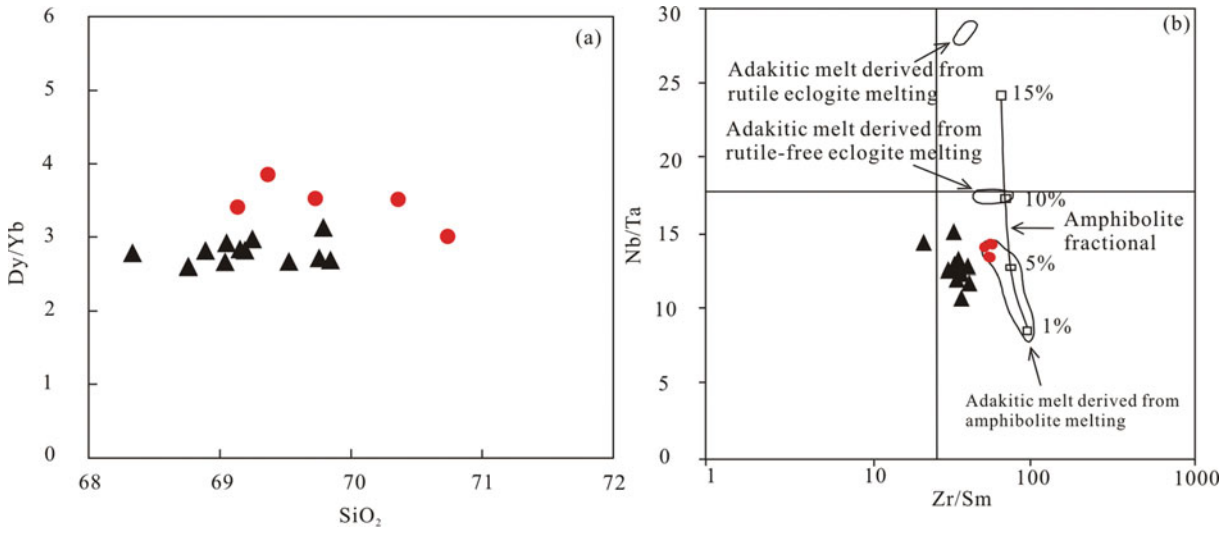

Figure 9. (Colour online) Plots of (a) Dy/Yb versus SiO_2 and (b) Nb/Ta versus Zr/Sm for the felsic rocks of study area. After Foley, Tiepolo & Vannucci (2002).

fractional crystallization of a hydrous basaltic magma. The low-pressure fractional crystallization of plagioclase and hornblende can generate concave REE patterns between the HREEs and the middle rare Earth elements (MREEs), leading to a decrease in Dy/Yb ratios with increasing SiO_2 concentrations (Castillo, Janney & Solidum, 1999; Macpherson, Dreher & Thirwall, 2006), although the adakitic rocks within the Haertaolegai pluton do not have either of these characteristics (Figs 6a, 9a). In addition, plotting the samples analysed during this study in a La/Sm versus La diagram (Fig. 10a) suggests that their evolution was mainly controlled by partial melting. This result, combined with a lack of Eu anomalies and a negative correlation between Na_2O and La with SiO_2 concentrations, suggests the Haertaolegai adakitic rocks were not derived by fractional crystallization of a basaltic magma (Castillo, Janney & Solidum, 1999; Macpherson, Dreher & Thirwall, 2006; Zhu *et al.* 2008).

The adakitic rocks in the study area have high Sr concentrations and Sr/Y ratios, low Y, Yb, and HREE concentrations and do not have visible Eu anomalies, indicating the presence of residual garnet and the absence of plagioclase in the source region for the magmas that formed these rocks (Rapp, Xiao & Shimizu, 2002; Xiong, Adam & Green, 2005). However, these rocks also have flat HREE patterns that indicate that amphibole had a more important role than garnet in the generation of the adakitic melts that formed these intrusions (Fig. 6a; Moyen, 2009; Huang & He, 2010). In addition, the low Nb/Ta ratios of these rocks are consistent with formation from adakitic melts derived from the melting of amphibolite material (Fig. 9b; Foley, Tiepolo & Vannucci, 2002; Xiong, 2006), and these samples plot close to adakitic melts derived from the melting of thickened mafic lower crustal material within a SiO_2 versus MgO diagram (Fig. 10b; Karsli *et al.* 2010). This suggests that the adakitic rocks in the study area formed from magmas generated by the melting of garnet-bearing amphibolite material within a thickened region of the mafic lower crust.

The Hf isotopic compositions of zircons within adamellites in the study area can also provide constraints on the nature of this thickened region of the mafic lower crust. Zircons within the adamellite have $\varepsilon Hf(t)$ values of +1.0 to +2.7 and T_{DM2} ages of 1032–1128 Ma, indicating that these magmas could have formed from a thickened region of the mafic lower crust that accreted during Mesoproterozoic time.

5.d. Tectonic setting of magmatism and implications for regional geology

The timing of the final closure of the Paleo-Asian Ocean within the western part of Inner Mongolia remains controversial, with previous research on the geochronology and geochemistry of Permian – Early Triassic ultramafic–mafic rocks in this area suggesting the presence of an intra-oceanic arc–trench system with multiple south- and north-directed subduction zones between 530 and 250 Ma. This system collided along the Solonker suture zone during late Permian – Middle Triassic time (Chen *et al.* 2000; Xiao *et al.* 2003, 2009; Jian *et al.* 2008; Chen, Jahn & Tian, 2009; Jian, Liu & Kröner, 2010). However, other research has suggested that the oceanic basin along the northern margin of the North China Plate disappeared during Late Devonian – early Carboniferous time, as evidenced by the age of the youngest ophiolite identified to date (>350 Ma; Shao, 1991; Tang, 1992; Zhang, Zhou & Wang, 2003). Although a Permian ophiolite has been identified within the Solon and Hegen mountains (Jian *et al.* 2008; Miao *et al.*, 2008), the presence of a widely distributed bimodal volcanic suite and A-type granite rocks to the north and south of the Solon and Hegen mountains is inconsistent with the subduction of oceanic crust during early Permian time in this area (Hong *et al.* 1994; Shi *et al.* 2004; Zhang & Jiang,

https://doi.org/10.1017/S0016756815000138 Published online by Cambridge University Press

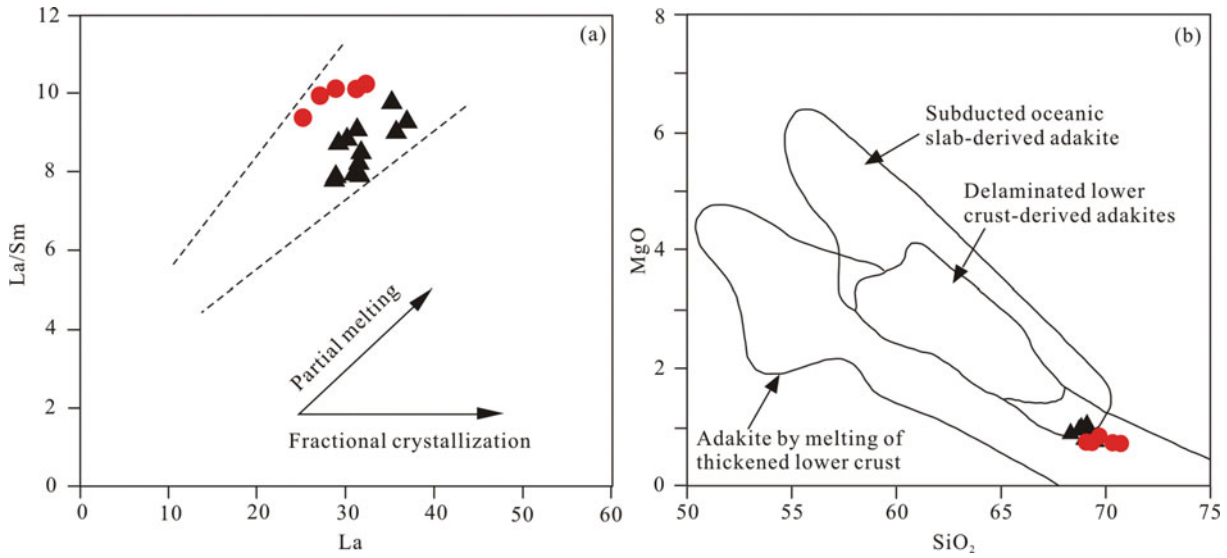

Figure 10. (Colour online) Plots of (a) La/Sm versus La and (b) MgO versus SiO_2 for the adamellites and granitic porphyries in study area. After Karsli *et al.* (2010).

2008; Luo, Wu & Zhao, 2009). This suggests that this Permian ophiolite formed within a remnant ocean or a continental rift (Li, 2006; Zhang & Jiang, 2008). Xu *et al.* (2014) also propose that the Permian ophiolite in Solonker belongs to continental-margin-type ophiolite, the tectonic emplacement of which is associated with nappe structure but not oceanic crust subduction. In addition, the presence of an unconformity between Upper Devonian sediments and underlying rocks, and the differing styles of deformation between these units, led Tang (1990) and Xu *et al.* (2013) to suggest that the Paleo-Asian Ocean closed during Late Devonian time. Palaeomagnetic data also indicate that the North China and Mongolia blocks were amalgamated during Late Devonian – Permian time. Palaeomagnetic evidence suggests that the closure of the Paleo-Asian Ocean occurred previously to Late Devonian time (Zhao *et al.* 2013) and that central Inner Mongolia was part of the NCC during late Carboniferous – early Permian time (Li *et al.* 2012). The discovery of early–middle Permian Cathaysian flora (Zhou *et al.* 2010) north of the Erenhot–Hegenshan fault also indicates that the Paleo-Asian Ocean disappeared before early Permian time. All the above corroborate the theory that the Paleo-Asian Ocean was closed at least from Late Devonian time.

Certain types of magmatic activity are of importance to constrain the evolution of the orogeny. Recent research has identified late Palaeozoic rocks in western Inner Mongolia that were generated during post-collisional magmatism. This is as exemplified by Tang *et al.* (2011), who recognized a late Carboniferous bimodal volcanic suite within the western part of the Hunshandake Block that most likely formed in an extensional setting after collision between the North China Craton and the South Mongolia microcontinent. Zhang *et al.* (2011*b*, 2014) also reported a bimodal high-K magmatic association with an A-type granite in the Bayinwula area. In addition the Kebu diorite massif in Urad Zhongqi (Luo, Wu & Li, 2007), within the northern margin of the North China Craton, is adakitic and yields a SHRIMP zircon age of 291 ± 4 Ma; this suggests that these units formed from magmas generated by partial melting of mafic lower continental crustal material during post-collisional basaltic underplating. A-type granites with ages of 276 and 277 Ma have been identified in the Xilinhaote area and to the south of Urad Zhongqi (Shi *et al.* 2004; Luo, Wu & Zhao, 2009), respectively, all of which formed during post-collisional magmatism. Zhao, Wu & Luo (2011) also identified a 269 Ma mafic–ultramafic pluton within the Wengeng and Urad Zhongqi areas, and suggested that this magmatism occurred in a post-collisional tectonic setting. The early Permian magmatic rocks from the northern NCC and the neighbouring orogenic belt constitute a magmatic province which exhibits temporal and spatial distribution, rock constituent, magma genesis and metamorphic style typical of post-collisional magmatism (Zhang *et al.* 2011*a*). Jahn *et al.* (2009) also suggested that the voluminous early Permian peralkaline and alkaline granitoids and genetically related bimodal volcanics emplaced in the eastern CAOB occurred in an extensional tectonic setting.

In summary, these studies suggest that the Paleo-Asian Ocean in western Inner Mongolia closed prior to early Permian time, confirming studies from a wider area of the CAOB (Hong *et al.* 2004; Jahn *et al.* 2009). To determine the precise time of the final closure of the Paleo-Asian Ocean, more research and evidence are required.

The felsic rocks in the study area are dominated by adamellite and porphyritic granite phases, both of which have low A/CNK ratios that are indicative of metaluminous granites (Fig. 5b). These samples have primitive-mantle-normalized multi-element variation patterns that are LILE enriched and HFSE (e.g. Nb,

https://doi.org/10.1017/S0016756815000138 Published online by Cambridge University Press

P, and Ti) depleted, similar to typical post-collisional I-type granites (Kuster & Harms, 1998). These felsic rocks are also adakitic and formed from magmas generated by partial melting of a thickened region of the mafic lower crust. The contemporaneous nature of mafic and felsic rocks in the study area is indicative of a bimodal igneous rock association that most likely formed in an extensional setting. This suggests that the Haertaolegai adakitic rocks and the associated gabbroic diorites formed during the transition from collisional compression to post-collisional extension, indicating in turn that the Paleo-Asian Ocean in western Inner Mongolia closed before early Permian time.

These data, combined with the geology of this region and our new knowledge of the petrogenesis of mafic and felsic rocks in the study area, allows the construction of the following genetic model for the Haertaolegai bimodal intrusive rocks. The early Permian continental collision of the South Mongolia microcontinent with the North China Craton caused a region of juvenile mafic lower crust to undergo tectonic thickening and metamorphism into garnet-bearing amphibolite material. Slab break-off caused asthenospheric mantle material to ascend, resulting in partial melting of the juvenile mafic lower crust and generating the magmas that formed the Haertaolegai adakitic intrusions. The upwelling asthenospheric material also provided sufficient heat energy to melt the lithospheric mantle, generating voluminous mafic magmas that formed the mafic rocks in the study area.

6. Conclusions

(1) A suite of bimodal intrusive rocks within western Inner Mongolia includes mafic intrusions that yield LA-ICP-MS zircon U–Pb dates of *c.* 286 Ma and felsic intrusions that were emplaced between 286 and 300 Ma.

(2) The primary magma that formed the early Permian mafic rocks was generated by partial melting of lithospheric mantle material that was previously modified by subduction-related fluids. The felsic rocks are adakitic and formed from primary magmas generated by partial melting of a thickened region of juvenile mafic lower crust.

(3) The late Carboniferous – early Permian bimodal intrusive rocks in western Inner Mongolia formed during the transition from collisional compression to post-collisional extension, indicating that the Paleo-Asian Ocean in western Inner Mongolia closed before 300 Ma.

Acknowledgements. We thank the staff of the State Key Laboratory of Continental Dynamics, Northwestern University, Xi'an, China; the State Key Laboratory of Geological Processes and Mineral Resources, China University of Geosciences, Wuhan, China; and Geological Analysis and Research Centre of Nuclear Industry of China for their assistance during U–Pb zircon dating, Hf isotope analyses and major and trace element analyses. This study was supported by Research Program 'Au-Co-Ni Mineralization potential estimation of Tugurige gold mine and periphery in Urad Zhongqi, Inner Mongolia' from Geological Brigade No. 208 of China National Nuclear Corporation. We are grateful to Gengxin Zhang and Guoyu Shao of the Geological Brigade No. 208 of China National Nuclear Corporation for their help during the field investigations. The helpful and constructive reviews and suggestions by Professor W.J. Xiao and an anonymous reviewer are greatly appreciated.

References

ABE, N., ARAI, S. & YURIMOTO, H. 1998. Geochemical characteristics of the uppermost mantle beneath the Japan island arcs: Implications for upper mantle evolution. *Physics of the Earth and Planetary Interiors* **107**, 233–48.

ANDERSEN, T. 2002. Correction of common lead in U–Pb analyses that do not report ^{204}Pb. *Chemical Geology* **192**, 59–79.

ATHERTON, M. P. & PETFORD, N. 1993. Generation of sodium-rich magmas from newly underplated basaltic crust. *Nature* **362**, 144–6.

BADARCH, G., CUNNINGHAM, W. D. & WINDLEY, B. F. 2002. A new terrane subdivision for Mongolia: implications for the Phanerozoic crustal growth of Central Asia. *Journal of Asian Earth Sciences* **21**, 87–104.

BLICHERT-TOFT, J., CHAUVEL, C. & ALBARÈDE, F. 1997. Separation of Hf and Lu for high-precision isotope analysis of rock samples by magnetic sector-multiple collector ICP-MS. *Contributions to Mineralogy and Petrology* **127**, 248–60.

BOYNTON, W. V. 1984. Geochemistry of the rare earth elements: meteorite studies. In *Rare Earth Element Geochemistry* (ed. P. Henderson), pp. 63–114. Amsterdam: Elsevier.

CASTILLO, P. R., JANNEY, P. E. & SOLIDUM, R. U. 1999. Petrology and geochemistry of Camiguin island, southern Philippines: insights to the source of adakites and other lavas in a complex arc setting. *Contributions to Mineralogy and Petrology* **134**, 33–51.

CHEN, B., JAHN, B. M. & TIAN, W. 2009. Evolution of the Solonker suture zone: constraints from zircon U–Pb ages, Hf isotopic ratios and whole-rock Nd–Sr isotope compositions of subduction- and collision-related magmas and forearc sediments. *Journal of Asian Earth Sciences* **34**, 245–57.

CHEN, B., JAHN, B. M., WILDE, S. & XU, B. 2000.Two contrasting Paleozoic magmatic belts in northern Inner Mongolia, China: petrogenesis and tectonic implications. *Tectonophysics* **328**, 157–82.

CHEN, L. H. & ZHOU, X. H. 2004. Ultramafic xenoliths in Mesozoic diorite in West Shan Dong Province. *Science in China (Series D)* **47**(6), 489–99.

DAVIS, G. A., ZHENG, Y., WANG, C., DARBY, B. J., ZHANG, C. & GEHRELS, G. E. 2001. Mesozoic tectonic evolution of the Yanshan Fold and Thrust Belt, with emphasis on Hebei and Liaoning provinces, Northern China. In *Paleozoic and Mesozoic Tectonic Evolution of Central and Eastern Asia: From Continental Assembly to Intracontinental Deformation* (eds M. S. Hendrix & G. A. Davis), pp. 171–97. Geological Society of America, Memoir no. 194.

DEFANT, M. J. & DRUMMOND, M. S. 1990. Derivation of some modern arc magmas by melting of young subducted lithosphere. *Nature* **347**, 662–5.

DONG, Y. P., LIU, X. M., SANTOSH, M., CHEN, Q., ZHANG, X. N., LI, W., HE, D. F. & ZHANG, G. W. 2012. Neoproterozoic accretionary tectonics along the northwestern

https://doi.org/10.1017/S0016756815000138 Published online by Cambridge University Press

margin of the Yangtze Block, China: Constraints from zircon U–Pb geochronology and geochemistry. *Precambrian Research* **196–197**, 247–74.

EILER, J. M., CRAWFORD, A., ELLIOTT, T., FARLEY, K. A., VALLEY, J. W. & STOLPER, E. M. 2000. Oxygen isotope geochemistry of oceanic arc lavas. *Journal of Petrology* **41**(2), 229–56.

FISHER, C. M., VERVOORT, J. D. & HANCHAR, J. M. 2014. Guidelines for reporting zircon Hf isotopic data by LA-MC-ICPMS and potential pitfalls in the interpretation of these data. *Chemical Geology* **363**, 125–33.

FOLEY, S., TIEPOLO, M. & VANNUCCI, R. 2002. Growth of early continental crust controlled by melting of amphibolite in subduction zones. *Nature* **417**, 837–40.

FREY, F. A. & PRINZ, M. 1978. Ultramafic inclusions from San Carlos, Arizona: petrologic and geochemical data bearing on their petrogenesis. *Earth and Planetary Science Letters* **38**, 129–76.

GAO, J., KLEMD, R., LONG, L. L., XIONG, X. M. & QIAN, Q. 2009. Adakitic signature formed by fractional crystallization: an interpretation for the Neo-Proterozoic metaplagiogranites of the NE Jiangxi ophiolitic melange belt, South China. *Lithos* **110**, 277–93.

GAO, S., LUO, T. C., ZHANG, B. R., ZHANG, H. F., HAN, Y. W., ZHAO, Z. D. & HU, Y. K. 1998. Chemical composition of the continental crust as revealed by studies in East China. *Geochimica et Cosmochimica Acta* **62**, 1959–75.

GAO, S., RUDNICK, R. L., YUAN, H. L., LIU, X. M., LIU, Y. S., XU, W. L., LING, W. L., AYERS, J., WANG, X. C. & WANG, Q. H. 2004. Recycling lower continental crust in the North China craton. *Nature* **432**(7019), 892–7.

GROVE, T. L., ELKINS TANTON, L. T., PARMAN, S. W., CARTTERJEE, N., MUNTENER, O. & GAETANI, G. A. 2003. Fractional crystallization and mantle melting controls on calk-alkaline differentiation trends. *Contributions to Mineralogy and Petrology* **145**(5), 515–33.

HEUBECK, C. 2001. Assembly of central Asia during the middle and late Paleozoic. In *Paleozoic and Mesozoic Tectonic Evolution of Central Asia: From Continental Assembly to Intra Continental Deformation* (eds M. S. Hendrix & G. A. Davis), pp. 1–22. Geological Society of America, Memoir no. 194.

HOFMANN, A. W. 1988. Chemical differentiation of the Earth: the relationship between mantle, continental crust, and oceanic crust. *Earth and Planetary Science Letters* **90**, 297–314.

HONG, D. W., HUANG, H. Z., XIAO, Y. J., XU, H. & JIN, M. 1994. The Permian alkaline granites in central Inner Mongolia and their geodynamic significance. *Acta Geological Sinica* **68**(3), 219–230 (in Chinese with English abstract).

HONG, D. W., ZHANG, J. S., WANG, T., WANG, S. G. & XIE, X. L. 2004. Continental crustal growth and the supercontinental cycle: evidence from the Central Asian Orogenic Belt. *Journal of Asian Earth Sciences* **23**, 799–813.

HOSKIN, P. W. & SCHALTEGGER, U. 2003. The composition of zircon and igneous and metamorphic petrogenesis. *Reviews in Mineralogy and Geochemistry* **53**(1), 27–62.

HU, Z. C., LIU, Y. S., GAO, S., LIU, W. G., YANG, L., ZHANG, W., TONG, X. R., LIN, L., ZONG, K. Q., LI, M., CHEN, H. H. & ZHOU, L. 2012. Improved in situ Hf isotope ratio analysis of zircon using newly designed X skimmer cone and jet sample cone in combination with the addition of nitrogen by laser ablation multiple collector ICP–MS. *Journal of Analytical Atomic Spectrometry* **27**(9), 1391–9.

HUANG, F. A. & HE, Y. S. 2010. Partial melting of the dry mafic continental crust: implications for petrogenesis of C-type adakites. *Chinese Science Bulletin* **55**, 2428–39.

IRVINE, T. H. & BARAGAR, W. R. A. 1971. A guide to the chemical classification of the common volcanic rocks. *Canadian Journal of Earth Sciences* **8**(5), 523–48.

JAHN, B. M. 2004. The Central Asian Orogenic Belt and growth of the continental crust in the Phanerozoic. In *Aspects of the Tectonic Evolution of China* (eds J. Malpas, C. J. N. Fletcher, J. R. Ali & J. C. Aitchison), pp. 73–100. Geological Society of London, Special Publication no. 226.

JAHN, B. M., LITIVNOVSKY, B. A., ZANVILEVICH, A. N. & REICHOW, M. 2009. Peralkaline granitoid magmatism in the Mongolian–Transbaikalian Belt: evolution, petrogenesis and tectonic significance. *Lithos* **113**, 521–39.

JAHN, B. M., WU, F. Y. & CHEN, B. 2000. Granitoids of the Central Asian orogenic belt and continental growth in the Phanerozoic. *Transactions of the Royal Society of Edinburgh: Earth Sciences* **91**, 181–93.

JIAN, P., LIU, D. & KRÖNER, A. 2010. Evolution of a Permian intraoceanic arc-trench system in the Solonker suture zone, Central Asian Orogenic Belt, China and Mongolia. *Lithos* **118**, 169–90.

JIAN, P., LIU, D., KRÖNER, A., WINDLEY, B. F., SHI, Y., ZHANF, F., SHI, G., MIAO, L., ZHANG, W., ZHANG, Q., ZHANG, L. & REN, J. 2008. Time scale of an early to mid-Paleozoic orogenic cycle of the long-lived Central Asian Orogenic Belt, Inner Mongolia of China: implications for continental growth. *Lithos* **101**, 233–59.

KARSLI, O., DOKUZ, A., UYSAL, I., AYDIN, F., KANDEMIR, R. & WIJBRANS, J. 2010. Generation of the Early Cenozoic adakitic volcanism by partial melting of mafic lower crust, Eastern Turkey: implications for crustal thickening to delamination. *Lithos* **114**, 109–20.

KAY, R. W. & KAY, S. M. 1993. Delamination and delamination magmatism. *Tectonophysics* **219**, 177–89.

KUSTER, D. & HARMS, U. 1998. Post-collisional potassic granitoids from the southern and northwestern parts of the late Neo-proterozoic East African Orogen: A review. *Lithos* **45**, 177–95.

LI, J. Y. 2006. Permian geodynamic setting of Northeast China and adjacent regions: closure of the Paleo-Asian Ocean and subduction of the Paleo-Pacific Plate. *Journal of Asian Earth Sciences* **26**, 207–24.

LI, P. W., ZHANG, S. H., GAO, R., LI, H. Y., ZHAO, Q. L., LI, Q. S. & GUAN, Y. 2012. New Upper Carboniferous–Lower Permian paleomagnetic results from the central Inner Mongolia and their geological implications. *Journal of Jilin University (Earth Sciences Edition)* **S1**, 423–34 (in Chinese with English abstract).

LIU, Y. S., HU, Z. C., GAO, S., GÜNTHER, D., XU, J., GAO, C. G. & CHEN, H. H. 2008. In situ analysis of major and trace elements of anhydrous minerals by LA-ICP-MS without applying an internal standard. *Chemical Geology* **257**, 34–43.

LIU, Y. S., HU, Z. C., ZONG, K. Q., GAO, C. G., GAO, S., XU, J. & CHEN, H. H. 2010. Reappraisement and refinement of zircon U–Pb isotope and trace element analyses by LA-ICP-MS. *Chinese Science Bulletin* **55**, 1535–46.

LUDWIG, K. R. 2003. *Isoplot/Ex, Version 3: A Geochronological Toolkit for Microsoft Excel*. California: Geochronology Centre Berkeley.

LUO, H. L., WU, T. R. & LI, Y. 2007. Geochemistry and SHRIMP dating of the Kebu massif from Wulatezhongqi, Inner Mongolia: evidence for the Early Permian underplating beneath the North China Craton. *Acta Petrologica Sinica* **23**, 755–66 (in Chinese with English abstract).

LUO, H. L., WU, T. R. & ZHAO, L. 2009. Zircon SHRIMP U–Pb dating of Wuliangsitai A-type granite on the northern margin of the North China plate and tectonic significance. *Acta Petrologica Sinica* **25**, 515–26 (in Chinese with English abstract).

MACPHERSON, C. G., DREHER, S. T. & THIRWALL, M. F. 2006. Adakites without slab melting: high pressure differentiation of island arc magma, Mindanao, the Philippines. *Earth and Planetary Science Letters* **243**, 581–93.

MANIAR, P. D. & PICCOLI, P. M. 1989. Tectonic discrimination of granitoids. *Geological Society of America Bulletin* **101**(5), 635–43.

MARTIN, H. 1999. Adakitic magmas: modern analogues of Archaean granitoids. *Lithos* **46**, 411–29.

MARTIN, H., SMITH, R. H., RAPP, R., MOYEN, J. F. & CHAMPION, D. 2005. An overview of adakite, tonalite–trondhjemite–granodiorite (TTG), and sanitoid: relationships and some implications for crustal evolution. *Lithos* **79**, 1–24.

MIAO, L., FAN, W., LIU, D., ZHANG, F., SHI, Y. & GUO, F. 2008. Geochronology and geochemistry of the Hegenshan ophiolitic complex: Implications for late-stage tectonic evolution of the Inner Mongolia-Daxinganling Orogenic Belt, China. *Journal of Asian Earth Sciences* **32**, 348–70.

MOYEN, J. F. 2009. High Sr/Y and La/Yb ratios: the meaning of the "adakitic signature". *Lithos* **112**, 556–74.

PECCERILLO, A. & TAYLOR, S. R. 1976. Geochemistry of Eocene calc-alkaline volcanic rocks from the Kastamonu area, Northern Turkey. *Contributions to Mineralogy and Petrology* **58**(1), 63–81.

QU, X. M., HOU, Z. Q. & LI, Y. G. 2004. Melt components derived from a subducted slab in late orogenic ore-bearing porphyries in the Gangdese copper belt, southern Tibetan plateau. *Lithos* **74**, 131–48.

RAPP, R. P. & WATSON, E. B. 1995. Dehydration melting of metabasalt at 8–32Kbar: implications for continental growth and crust-mantle recycling. *Journal of Petrology* **36**, 891–931.

RAPP, R. P., XIAO, L. & SHIMIZU, N. 2002. Experimental constraints on the origin of potassium-rich adakites in eastern China. *Acta Petrologica Sinica* **18**, 293–302.

RUDNICK, R. L. & GAO, S. 2003. Composition of the continental crust. *Treatise in Geochemistry* **3**, 1–64.

SAJONA, F. G., MAURY, R. C., PUBELLIER, M., LETERRIER, J., BELLON, H. & COTTON, J. 2000. Magmatic source enrichment by slab-derived melts in a young post-collision setting, central Mindanao(Philippines). *Lithos* **54**(3–4), 173–206.

ŞENGÖR, A. M. C. & NATAL'IN, B. A. 1996. Paleotectonics of Asia: fragments of a synthesis. In *The Tectonic Evolution of Asia* (eds A. Yin & T. M. Harrison), pp. 486–640. Cambridge, UK: Cambridge University Press.

ŞENGÖR, A. M. C., NATAL'IN, B. A. & BURTMAN, V. S. 1993. Evolution of the Altaid tectonic collage and Paleozoic crustal growth in Eurasia. *Nature*, **364**, 299–307.

SEO, J., CHOI, S. G. & OH, C. W. 2010. Petrology, geochemistry, and geochronology of the post-collisional Triassic mangerite and syenite in the Gwangcheon area, Hongseong Belt, South Korea. *Gondwana Research* **18**, 479–96.

SHAO, J. A. 1991. *Crust Evolution in the Middle Part of the Northern Margin of Sino-Korean Plate*. Beijing: Peking University Press, 136 pp. (in Chinese with English abstract).

SHI, G. H., MIAO, L. C., ZHANG, F. Q., JIAN, P., FAN, W. M. & LIU, D. Y. 2004. The age and its regional tectonic implication of the Xilinhot A-type granites, Inner Mongolia. *Chinese Science Bulletin* **49**, 384–9.

SMITHIES, R. H. 2000. The Archean tonalite–trondhjemite–granodiorite (TTG) series is not an analogue of Cenozoic adakite. *Earth and Planetary Science Letters* **182**, 115–25.

SUN, S. S. & MCDONOUGH, W. F. 1989. Chemical and isotopic systematics of oceanic basalts: implications for mantle composition and processes. In *Magmatism in Ocean Basins* (eds A. D. Saunders & M. J. Norry), pp. 313–345. Geological Society of London, Special Publication no. 42.

TANG, K. D. 1990. Tectonic development of Paleozoic fold belts at the north margin of the Sino–Korean craton. *Tectonics* **9**, 249–60.

TANG, K. D. 1992. *Tectonic Evolution and Minerogenetic Regularities of the Fold Belt along the Northern Margins of Sino-Korean Plate*. Beijing: Peking University Press. 277 pp. (in Chinese with English abstract).

TANG, W. H., ZHANG, Z. C., LI, J. F., FENG, Z. S. & CHEN, C. 2011. Geochemistry of the Carboniferous volcanic rocks of Benbatu Formation in Sonid Youqi, Inner Mongolia and its geological significance. *Acta Scientiarum Naturalium Universitatis Pekinensis* **47**, 321–30.

TAYLOR, S. R. & MCLENNAN, S. 1995. The geochemical composition of the continental crust. *Reviews of Geophysics* **33**, 241–65.

WANG, Q. & LIU, X. Y. 1986, Paleoplate tectonics between Cathaysia and Angaraland in Inner Mongolia of China. *Tectonics* **5**, 1073–88.

WANG, Q., MCDERMOTT, F., XU, J. F., BELLON, H. & ZHU, Y. T. 2005. Cenozoic K-rich adakitic volcanic rocks in the Hohxil area, northern Tibet: Lower-crustal melting in an intracontinental setting. *Geology* **33**(6), 465–8.

WANG, Y. 1996. *Tectonic Evolutional Processes of Inner Mongolia-Yanshan Orogenic Belt in Eastern China during the Late Paleozoic–Mesozoic*. Beijing: Geological Publishing House (in Chinese).

WAREHAM, C. D., MILLAR, I. L. & VAUGHAN, A. P. M. 1997. The generation of sodic granitic magmas, western Palmer Land, Antarctic Peninsula. *Contributions to Mineralogy and Petrology* **128**(1), 81–96.

WILSON, W. 1989. *Igneous Petrogenesis*. London: Unwin Hyman, pp. 327–73.

WINDLEY, B. F., ALEXEIEV, D., XIAO, W. J., KRÖNER, A. & BADARCH, G. 2007. Tectonic models for accretion of the Central Asian Orogenic Belt. *Journal of the Geological Society of London* **164**, 31–47.

XIAO, W. J., WINDLEY, B., HAO, J. & ZHAI, M. G. 2003. Accretion leading to collision and the Permian Solonker suture, Inner Mongolia, China: termination of the Central Asian Orogenic Belt. *Tectonics* **22**, 1069–89.

XIAO, W. J., WINDLEY, B. F., HUANG, B. C., HAN, C. M., YUAN, C., CHEN, H. L., SUN, M., SUN, S. & LI, J. L. 2009. End-Permian to mid-Triassic termination of the accretionary processes of the southern Altaids: implications for the geodynamic evolution, Phanerozoic continental growth, and metallogeny of Central Asia. *International Journal of Earth Science* **98**, 1189–287.

XIONG, X. L. 2006. Trace element evidence for growth of early continental crust by melting of rutile-bearing hydrous eclogite. *Geology* **34**, 945–8.

XIONG, X. L., ADAM, J. & GREEN, T. H. 2005. Rutile stability and rutile/melt HFSE partitioning during partial melting of hydrous basalt: implications for TTG genesis. *Chemical Geology* **218**, 339–59.

XU, B. & CHARVET, J. 2010. Mid-Paleozoic opposite Orogenic Belt in Inner Mongolia of China and its

significance for Central Asian Orogenic Belt. International Association for Gondwana Research Conference Series 9, Qingdao, China, Abstract Volume, p. 84.

XU, B., CHARVET, J., CHEN, Y., ZHAO, P. & SHI, G. Z. 2013. Middle Paleozoic convergent orogenic belts in western Inner Mongolia (China): Framework, kinematics, geochronology and implications for tectonic evolution of the Central Asian Orogenic Belt. *Gondwana Research* **23**(4), 1342–64.

XU, B. & CHEN, B. 1993. The opposite subduction and collision between the Siberian and Sino-Korean plates during the early-middle Paleozoic. Report No: 4 of the IGCP Project 283: Geodynamic Evolution of Paleoasian Ocean, Novosibirsk, USSR, pp. 148–50.

XU, B. & CHEN, B. 1997. Framework and evolution of the middle Paleozoic orogenic belt between Siberian and North China Plates in northern Inner Mongolia. *Science in China, Series D* **40**, 463–9.

XU, B., LIU, S. W., WANG, C. Q., ZHENG, H. F. & TIAN, F. 2000. Sm–Nd, Rb–Sr geochronology of the Baoyintu Group in northwestern Inner Mongolia. *Geological Review* **46**, 86–90.

XU, B., ZHAO, P., BAO, Q. Z., ZHOU, Y. H., WANG, Y. Y. & LUO, Z. W. 2014. Preliminary study on the pre-Mesozoic tectonic unit division of the Xing-Meng Orogenic Belt (XMOB). *Acta Petrologica Sinica* **30**(7), 1841–57 (in Chinese with English abstract).

XU, J. F., SHINJIO, R., DEFANT, M. J., WANG, Q. & RAPP, R. P. 2002. Origin of Mesozoic adakitic intrusive rocks in the Ningzhen area of east China: partial melting of delaminated lower continental crust? *Geology* **12**, 1111–4.

YANG, J. H., WU, F. Y., SHAO, J. A., WILDE, S. A., XIE, L. W. & LIU, X. M. 2006. Constraints on the timing of uplift of the Yanshan Fold and Thrust Belt, North China. *Earth and Planetary Science Letters* **246**(3), 336–52.

YANG, J. H., WU, F. Y., WILDE, S. A. & ZHAO, G. C. 2008. Petrogenesis and geodynamics of Late Archeanmagmatismin eastern Hebei, eastern North China Craton: geochronological, geochemical and Nd–Hf isotopic evidence. *Precambrian Research* **167**, 125–49.

YANG, J. S., LIU, F. L., WU, C. L., XU, Z. Q., SHI, R., CHEN, S., DELOULE, E. & WOODEN, J. 2005. Two ultrahigh-pressure metamorphic events recognized in the central orogenic belt of China: evidence from the U–Pb dating of coesite-bearing zircons. *International Geology Review* **47**, 323–43.

YUAN, H. L., GAO, S., LIU, X. M., LI, H. M., GUNTHER, D. & WU, F. Y. 2004. Accurate U–Pb age and trace element determinations of zircon by laser ablation-inductively coupled plasma mass spectrometry. *Geostandards Newsletter* **28**, 353–70.

ZHANG, Q., WANG, Y., QIAN, Q., YANG, J. H., WANG, Y. L., ZHAO, T. P. & GUO, G. J. 2001. The characteristics and tectonic-metallogenic significances of the adakites in Yanshan Period from eastern China. *Acta Petrologica Sinica* **17**(2), 236–44 (in Chinese with English abstract).

ZHANG, Q., ZHOU, G. Q. & WANG, Y. 2003. The distribution of time and space of Chinese ophiolites, and tectonic settings. *Acta Petrologica Sinica* **19**(1), 1–8 (in Chinese with English abstract).

ZHANG, W. & JIAN, P. 2008. SHRIMP dating of Early Paleozoic granites from north Damaoqi, Inner Mongolia. *Acta Geologica Sinica* **82**, 778–87 (in Chinese with English abstract).

ZHANG, X. H., MAO, Q., ZHANG, H. F., ZHAI, M. G., YANG, Y. & HU, Z. 2011*a*. Mafic and felsic magma interaction during the construction of high-K calc-alkaline plutons within a metacratonic passive margin: the Early Permian Guyang batholith from the northern North China Craton. *Lithos* **125**, 569–91.

ZHANG, X. H., WILDE, S. A., ZHANG, H. F. & ZHAI, M. G. 2011*b*. Early Permian high-K calcalkaline volcanic rocks from northwest Inner Mongolia, North China: geochemistry origin and tectonic implications. *Journal of the Geological Society (London)* **168**, 153–71.

ZHANG, X. H., XUE, F. H., YUAN, L. L., MA, Y. G. & WILDE, S. A. 2012. Late Permian appinite–granite complex from northwestern Liaoning, North China craton: petrogenesis and tectonic implications. *Lithos* **155**, 201–17.

ZHANG, X. H., YUAN, L. L, XUE, F. H., YAN, X. & MAO, Q. 2014. Early Permian A-type granites from central Inner Mongolia, North China: magmatic tracer of post collisional tectonics and oceanic crustal recycling. *Gondwana Research*, published online 29 March 2014. doi: 10.1016/j.gr.2014.02.011.

ZHANG, X. H., ZHANG, H. F., WILDE, S. A., YANG, Y. H. & CHEN, H. H. 2010. Late Permian to Early Triassic mafic to felsic intrusive rocks from North Liaoning, North China: petrogenesis and implication for Phanerozoic continental growth. *Lithos* **117**, 283–306.

ZHAO, L., WU, T. R. & LUO, H. L. 2011. SHRIMP U-Pb dating, geochemistry and tectonic implications of the Beiqigetao gabbros in Urad Zhongqi area, Inner Mongolia. *Acta Petrologica Sinica* **27**(10), 3071–82 (in Chinese with English abstract).

ZHAO, P., CHEN, Y., XU, B., FAURE, M., SHI, G. Z. & CHOULET, F. 2013. Did the Paleo-Asian Ocean between North China Block and Mongolia Block exist during the Late Paleozoic? First paleomagnetic evidence from central-eastern Inner Mongolia, China. *Journal of Geophysical Research: Solid Earth* **118**, 1873–94.

ZHOU, Z. G., GU, Y. C., LIU, C. F., YU, Y. S., ZHANG, B., TIAN, Z. J., HE, P. B. & WANG, B. R. 2010. Discovery of early-middle Permian cathaysian flora Manduhubaolage area, Dong Ujinqin, Inner Mongolia, China and its geological significance. *Geological Bulletin of China* **28**, 21–5.

ZHU, D. C., ZHAO, Z. D., PAN, G. T., LEE, H. Y., KANG, Z. Q., LIAO, Z. L., WANG, L. Q., LI, G. M., DONG, G. C. & LIU, B. 2008. Early Cretaceous subduction-related adakite-like rocks of the Gangdese belt, southern Tibet: productions of slab melting and subsequent melt–peridotite interaction? *Journal of Asian Earth Sciences* **34**, 298–309.